Analysis of temporal variations of the polarization of Venus observed by Pioneer Venus orbiter.

Knibbe, W.J.J.; de Haan, J.F.; Hovenier, J.W.; Travis, L.D.

published in
Journal of Geophysical Research
1998

DOI (link to publisher)
10.1029/97JE03558

document version
Publisher's PDF, also known as Version of record

JOURNAL OF GEOPHYSICAL RESEARCH, VOL. 103, NO. E4, PAGES 8557–8574, APRIL 25, 1998

Analysis of temporal variations of the polarization of Venus observed by Pioneer Venus Orbiter

Willem Jan J. Knibbe,[1] Johan F. de Haan, and Joop W. Hovenier
Department of Physics and Astronomy, Free University, Amsterdam, Netherlands

Larry D. Travis
NASA Goddard Institute for Space Studies, New York

Abstract. Time variations of the disk-averaged polarization of Venus at wavelengths of 270, 365, 550, and 935 nm have been analyzed in terms of average haze optical thickness, cloud-top pressure, and cloud absorption optical thickness at 270 nm (presumably due to gaseous SO_2 absorption). The polarization data were deduced from observations made by the Pioneer Venus Orbiter between 1978 and 1990. Newton–Raphson iteration was used to derive the atmospheric parameter values from these observations. The required multiple scattering calculations were performed using the adding/doubling method. The atmospheric model consists of a cloud layer and a haze layer. The cloud and haze particles are composed of a concentrated sulfuric acid solution and have an effective radius of 1.05 μm and 0.25 μm, respectively. It was found that the disk-averaged haze optical thickness, cloud-top pressure, and cloud absorption optical thickness at 270 nm varied irregularly between 1978 and 1990. No trends were identified for the cloud-top pressure and cloud absorption optical thickness at 270 nm, but we did deduce a decrease in haze optical thickness during this 12 year period. Specific numbers are: (1) a haze optical thickness at 365 nm of about 0.25 in 1978 and less than 0.1 in 1990, (2) a cloud-top pressure that varies between 5 and 20 mbar, and (3) a cloud absorption optical thickness that varies between 0.0 and 4.0. Finally, our analysis revealed that the disk–averaged cloud-top pressure and haze optical thickness behaved anomalously in 1983.

1. Introduction

The visible clouds of Venus are mainly composed of sulfuric acid droplets and form a thick cover that completely obscures the planetary surface and lower cloud layers. These clouds have been extensively studied by polarimetry, spectrometry, and in situ probes. A number of these observations indicate that there are substantial temporal variations, particularly in the vertical structure of the cloud-top region.

A detailed analysis by *Hansen and Hovenier* [1974] of Earth-based polarimetry observations obtained before 1970 [*Dollfus*, 1966; *Coffeen and Gehrels*, 1969; *Dollfus and Coffeen*, 1970] indicated that a uniform cloud composed of concentrated sulfuric acid droplets with a narrow size distribution about a radius of 1.05 μm was required. However, polarimetry data from early in the mission of the Pioneer Venus Orbiter could be explained only with the addition of a "haze" of particles with radii of the order of 0.25 μm extending above the top of the larger particle cloud [*Kawabata et al.*, 1980]. Since the wavelength dependence of the refractive index deduced for these smaller haze particles was essentially identical to that of the cloud particles, the haze has been also identified as concentrated sulfuric acid. There had in fact been other observations which suggested a small-particle haze, specifically near-infrared spectrophotometry from 1970 to 1974 reported by *Martonchik and Beer* [1975] and Earth-based polarimetry at visual wavelengths from 1975 and 1977 [*Lane*, 1979; *Santer and Herman*, 1979], but the haze effects and corresponding amounts inferred from these studies were not as significant as those deduced by *Kawabata et al.* [1980]. A recent study by *Sato et al.* [1996] of Pioneer Venus polarization observations of the polar regions of Venus over the period 1979 to 1986 indicates that the polar haze optical thickness exhibits substantial short-term variations.

[1]Now at Transport Research Center, Ministry of Transport, Public Works and Water Management, Rotterdam, Netherlands.

Paper number 97JE03558.
0148-0227/98/97JE-03558$09.00

The spherical albedo of Venus at wavelengths shortward of 320 nm is found to show strong temporal variations [cf. *Barker et al.* 1975; *Travis*, 1975; *Moroz*, 1983]. According to *Tomasko et al.* [1980] and *Pollack et al.* [1980], these variations are most likely due to variations in the amount of absorbing material, probably SO_2, occurring within the upper part of the main clouds. Such a variation in amount of absorber would be expected to be manifest as well in the observed polarization at those wavelengths [*Travis*, 1975].

In their study of the Earth-based polarization observations of Venus, *Hansen and Hovenier* [1974] noted that the polarization at ultraviolet and the shorter visible wavelengths is more variable than at longer wavelengths. Most of this variation is attributable to changes in the cloud-top pressure level and the corresponding change in the relative contribution to the polarization by the Rayleigh scattering by gas molecules in the atmosphere above the cloud. Since the molecular scattering efficiency increases with decreasing wavelength, this effect on the observed polarization is most prominent at shorter wavelengths. By examining the polarization at wavelengths slightly longward of those at which the SO_2 absorption is important, this effect can be distinguished from that associated with variation in the absorber amount. Indeed, time variations in the cloud-top pressure have been deduced by *Coffeen and Hansen* [1974] and *Lane* [1979] from Earth-based polarization observations at 365 nm.

The polarization observations of Venus from the Pioneer Venus Orbiter mission cover a period of more than a decade, from orbit insertion in late 1978 through 1990, and as such provide an exceptional resource for examining temporal variations of the cloud and haze over a wide range of timescales. *Sato et al.* [1996] studied such time variations mainly for the polar regions of Venus between 1978 and 1986. This study is complementary to that of *Sato et al.* [1996] in various aspects. Here average properties of the entire disk are investigated for the entire time interval, up to 1990, which is important in the view of establishing long-term changes in the Venus atmosphere, and special attention is given to absorption properties at ultraviolet wavelengths, which might reveal relationships between the thickness of the haze layer and the amount of sulfur dioxide in the clouds. In an earlier paper [*Knibbe et al.*, 1997], we developed and applied a biwavelength analysis of Pioneer Venus polarization data to investigate spatial variations of Venus' cloud and haze properties at the beginning of the Pioneer Venus mission. In this paper we use essentially the same approach, namely, demanding agreement of the observations with the model calculations at two or three wavelengths, but the methodology is refined and is now based on Newton–Raphson iteration. Adopting a simple cloud-haze model, we retrieve the haze optical thickness, ultraviolet absorption optical thickness, and cloud-top pressure as the representative global average conditions for each map of the disk. Next, we examine the temporal variations of these average conditions over the complete time span of the observations.

2. Pioneer Venus Polarimetry Data

The Pioneer Venus Orbiter was launched in 1978 and carried on board the Cloud Photopolarimeter, among other instruments. Polarimetric observations were made from orbit insertion in 1978 through 1990, providing approximately 2000 detailed distributions of the polarization of Venus over the visible sunlit part of the disk. The observations were made in four wavelength bands, centered at 270, 365, 550, and 935 nm. See, e.g., *Colin and Hunten* [1977] and *Colin* [1980] for more information about the Pioneer Venus mission, and *Russell et al.* [1977] for more information about the photopolarimeter.

The polarimetric measurements have been reduced to tables containing values of the radiance I, degree of linear polarization P, and the angle of the direction of the polarization χ, as well as geometrical information. Following the terminology of *Kawabata et al.* [1980], we will refer to these tables as maps, where each map corresponds to one table containing observations of the visible sunlit part of the disk in four wavelengths.

In our analysis, we use values of the relative Stokes parameter q, which is calculated from I, P, and χ using the following well-known relations [e.g., *Chandrasekhar*, 1950; *Van de Hulst*, 1957; *Bohren and Huffman*, 1983; *Hovenier and Van der Mee*, 1983]:

$$P = \frac{\sqrt{Q^2 + U^2}}{I}, \tag{1}$$

$$\tan(2\chi) = \frac{U}{Q}, \tag{2}$$

where I, Q, and U are Stokes parameters. The Stokes parameters, as well as χ, are defined with respect to the local scattering plane. We adopt the convention that $\cos(2\chi)$ has the same sign as Q [*Hovenier and Van der Mee*, 1983]. It follows that

$$q = \frac{Q}{I} = P\cos(2\chi) = \frac{I_l - I_r}{I_l + I_r}, \tag{3}$$

where I_l and I_r are the radiances parallel and perpendicular to the reference plane, respectively [cf. *Chandrasekhar*, 1950]. The relative Stokes parameter q corresponds to the q component of the linear polarization. We ignore the u component, U/I, since with the local scattering plane as our choice for the reference plane, the u component is usually small. In particular, for the disk-averaged observations that we analyzed, the difference between P and $|q|$ is at most of the order of a few tenths of a percent. We note that, e.g., *Hansen and Hovenier* [1974] and *Kawabata et al.* [1980] employed $P_s = -q$ in their analyses of the linear polarization of Venus.

The measurement error in q at 365, 550, and 935 nm is about 0.002 per pixel, but about 0.01 at 270 nm. This larger error is due to the lower signal to noise ratio of the detectors at 270 nm [*Russell et al.*, 1977].

We did not employ the absolute radiance measurements I in our analysis, for the following reason. The detectors suffered from a continuous loss of sensitivity during the Pioneer Venus mission. Accurate information on the precise decline in sensitivity is unavailable. This sensitivity loss has, however, not affected the measurements of q, since this is a relative quantity.

The polarimetry maps of Venus were produced using the so-called spin-scan technique [e.g., *Russell et al.*, 1977] at disk-centered phase angles α_0 between 0° and about 160°. Here, α_0 denotes the angle between the directions from the sun to the center of the planet and from the center of the planet to the orbiter, at the moment that the center of the disk is observed. Phase angles at locations on the planet other than the center of the disk may differ up to about 7° from this value, as discussed by *Kawabata* [1981]. This is caused by the relatively short distance of the orbiter to the planetary surface, which ranged between about 22,000 and 66,000 km, in combination with the use of the spin-scan technique.

The polarimetric observations of Venus were performed by the Pioneer Venus Orbiter at values of α_0 which showed a regular variation in time. This variation is caused by the orbital motion of the planet Venus around the sun, which completes one orbit in its sidereal year of approximately 223 terrestrial days. Figure 1 shows α_0 as a function of time since the beginning of the mission. Clearly, α_0 increases monotonously during half a sidereal year, and after that decreases monotonously in the same period. The entire mission can be divided into about 40 such periods of half a Venusian sidereal year. Halfway through the Pioneer Venus mission, polarimetry was restricted to phase angles less than about 95° because of the declining power of the orbiter.

The polarimetry maps consist on average of about a thousand pixels for each wavelength. In order to focus on the temporal variations of globally averaged atmosphere properties, we have first added all values of Q and I for each map, and then computed

$$q = \frac{\sum_{i=1}^{N} Q_i}{\sum_{i=1}^{N} I_i}, \tag{4}$$

where Q_i and I_i denote values of Q and I for pixel i at a certain wavelength and N denotes the number of pixels of the map for that wavelength. Equatorial regions have a larger contribution per unit area to this average than polar regions. Further in this paper, the symbol q indicates disk-averaged values obtained according to (4). Values of q at 270 nm, 365 nm, 550 nm, and 935 nm will be labeled by letters approximately indicating colors corresponding to these wavelengths, namely, ultraviolet, blue, yellow, and red. Thus we write q_u, q_b, q_y, and q_r, respectively.

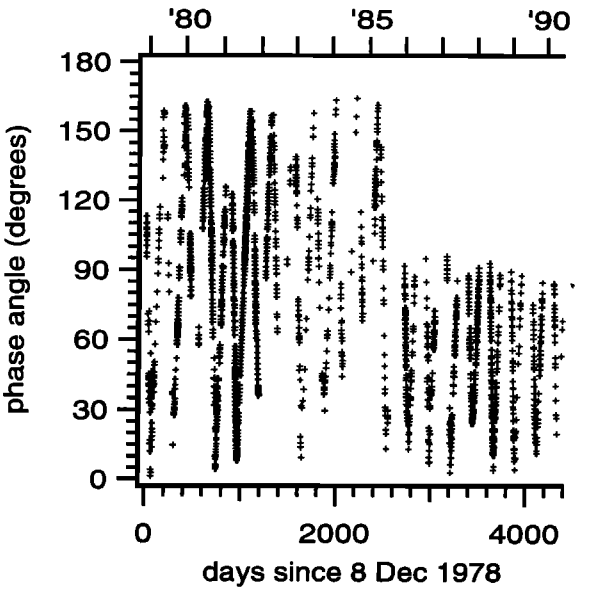

Figure 1. Disk-centered phase angles of Pioneer Venus polarimetry maps displayed as a function of the day on which the maps were made since the start at December 8, 1978.

Assuming random errors, measurement errors of the disk-averaged values of q are about an order of magnitude smaller than the errors per pixel, since the error decreases with the square root of the number of measurements.

As an example, Figure 2 shows q at the four different wavelengths at which observations were made as a function of α_0 for four periods of the Pioneer Venus mission each having a length of half a Venusian sidereal year. In Figure 2a, it is seen that, for phase angles less than 120°, q_u, as observed in 1979, is less negative than q_u as observed in later years, except for one observation at a phase angle of 113° in 1983. At phase angles larger than 140°, q_u as observed in 1979 is larger than q_u observed in later years. It appears that the observed values of q_u obtained in 1989, i.e., near the end of the Pioneer Venus mission, are generally closer to those obtained in 1981 than to those obtained in 1979. Further, this figure shows that the phase angle dependence of q_u as observed in 1983 is markedly different from the phase angle dependence of observations obtained in other years.

Figure 2b indicates that in 1979 q_b was less negative than in other years. Also, at this wavelength, the phase angle dependence of q_b observed in 1983 is very different from the dependences observed in other years. Further, the values obtained in 1989 are again closer to those obtained in 1981 than to those obtained in 1979.

Observations of q_y and q_r obtained in 1979, i.e., in the beginning of the Pioneer Venus mission, are different from observations obtained later in the mission.

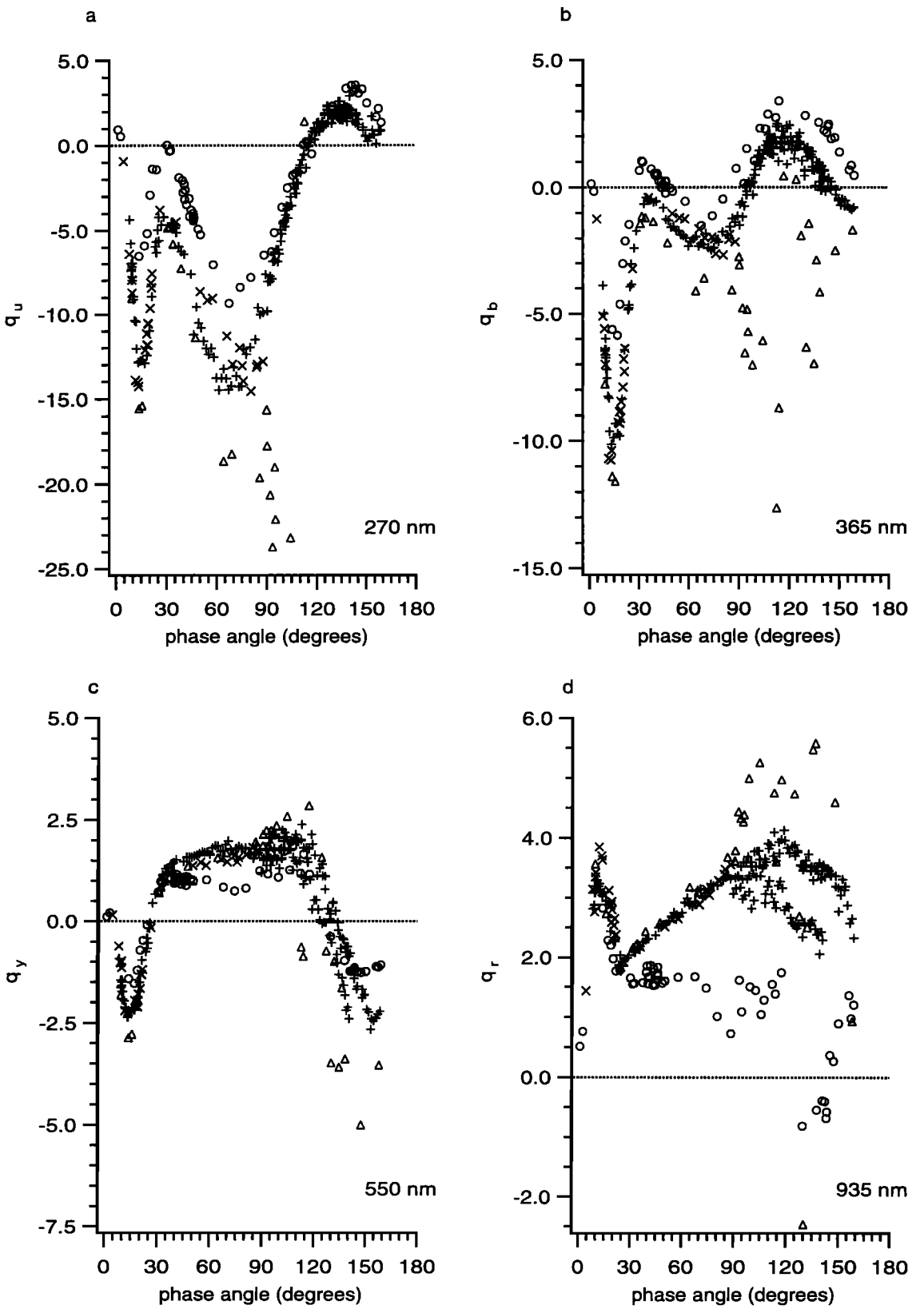

Figure 2. Observed values of q in percent as a function of phase angle for four wavelengths. The observations were made by the Pioneer Venus Orbiter during periods of half a Venusian sidereal year and started in February 1979 (circles), July 1981 (plus signs), May 1983 (triangles), and July 1989 (crosses), respectively. Each symbol corresponds to a disk-averaged value of q, as computed according to (4).

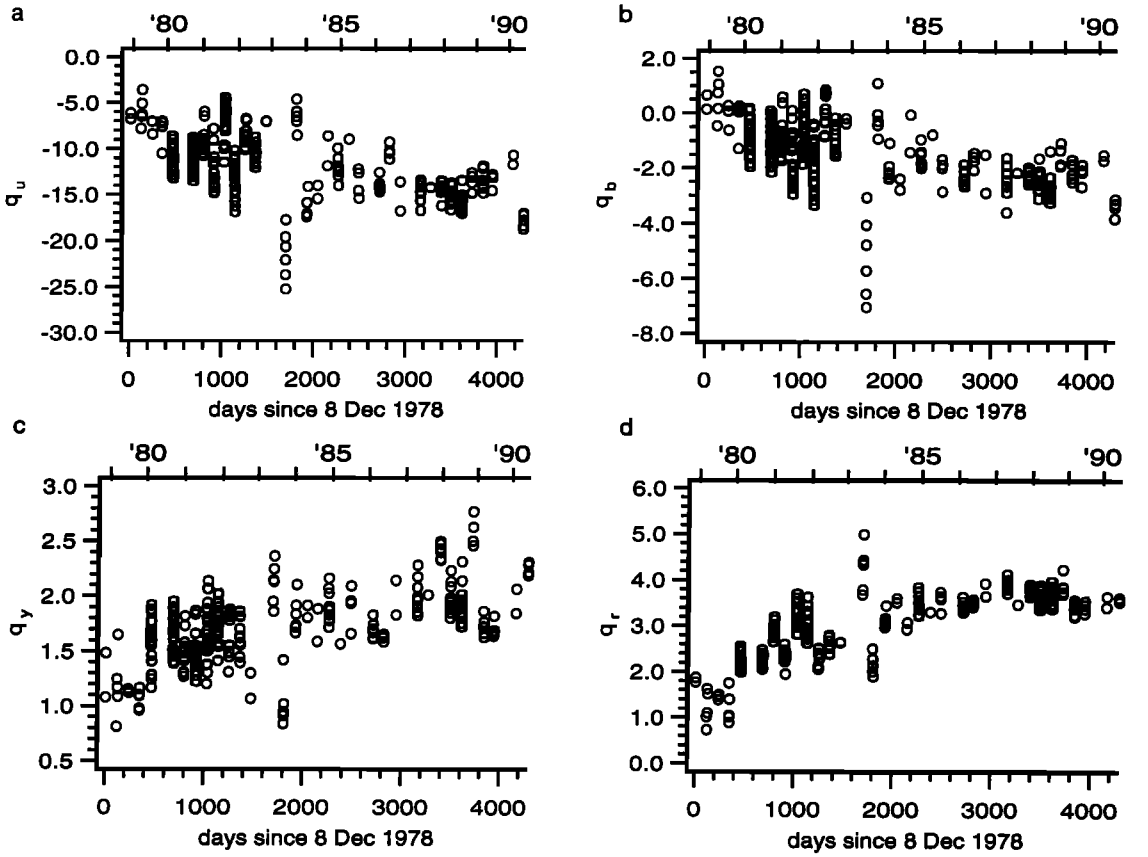

Figure 3. Observed values of q in percent as a function of time. Only observations made at phase angles between 80° and 100° are shown, made at (a) 270 nm, (b) 365 nm, (c) 550 nm, and (d) 935 nm.

This difference is more clearly visible for q_r than for q_y. At both wavelengths, there is little difference between observations of q_y and q_r obtained in 1981 and in 1989. Again, observations in 1983 show a markedly different phase angle dependence.

The observations of 1979 shown in Figure 2 are typical for observations obtained in the beginning of the Pioneer Venus mission, whereas the observations made in 1981 and 1989 indicate that there was only a modest amount of variation later in the mission. However, the observations made in 1983 are markedly different from observations made in all other periods. This was also found by *Sato et al.* [1996] for the polarization in polar regions of Venus as observed by the Pioneer Venus orbiter. In this paper, we concentrate on the interpretation of the gradual variation of q from values obtained in 1978 to values obtained in 1990 in terms of variations of haze optical thickness, cloud-top pressure, and absorption optical thickness at 270 nm. Therefore we will not pay special attention to the anomalous values obtained in 1983.

In order to reduce the computational labour, we analyzed only a selection from the Pioneer Venus polarization database. This selection covers the entire Pioneer Venus mission, and includes only maps made at disk-centered phase angles between 80° and 100°, since at these phase angles the influences of scattering molecules and haze particles on the linear polarization are both large, as will be shown in section 4. The time variations of q_u, q_b, q_y, and q_r observed at these phase angles are shown in Figure 3. The selection of 267 maps displayed in this figure was interpreted in terms of variations of atmosphere properties, as discussed further in this paper.

3. Model Atmosphere

To derive atmosphere properties from Pioneer Venus polarimetry observations, we performed calculations with the adding/doubling method, which is described by *De Haan et al.* [1987]. These calculations took into account all orders of scattering. In this section, the model atmosphere used for these calculations is described.

3.1. Vertical Structure

We used a two layered model of the atmosphere of Venus as schematically displayed in Figure 4. Both layers are locally plane parallel and homogeneously mixed.

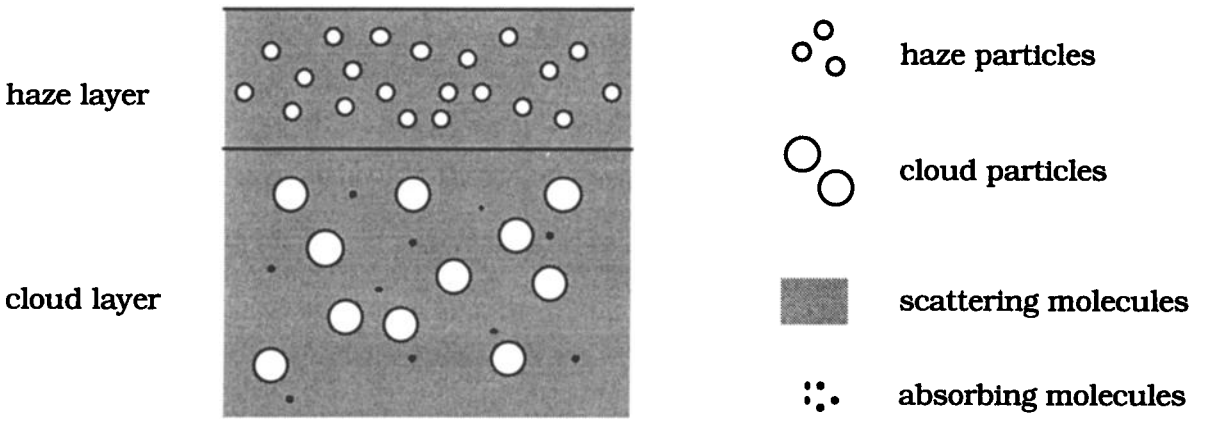

Figure 4. Schematic representation of the model for the atmosphere of Venus used in this paper. The upper layer is called haze layer and consists of haze particles and scattering molecules. The lower layer is called cloud layer and contains cloud particles as well as scattering and absorbing molecules.

Below these layers, a completely absorbing ground surface is present. The lower layer in this model corresponds to the main cloud deck. It contains scattering and absorbing molecules, and nonabsorbing cloud particles. The total optical thickness of this layer is the sum of the optical thicknesses of cloud particles, scattering molecules, and absorbing molecules, denoted by b_p^c, b_{sm}^c, and b_{am}^c, respectively. The upper layer contains nonabsorbing haze particles and scattering molecules. Their optical thicknesses are indicated by $b_p^h$and b_{sm}^h, respectively. Concerning scattering molecules, we employ a value of 0.079 for the molecular depolarization factor, after *Alms et al.* [1975] and *De Haan* [1987].

Absorbing matter within the haze layer is ignored in our model. This is in agreement with previous analyses of Pioneer Venus observations [*Tomasko et al.*, 1980; *Pollack et al.*, 1980], since these analyses indicated that absorbing material is mainly located in the lower portion of the so–called upper cloud, whereas the haze is at the top of the upper cloud.

We now discuss the values adopted for the above mentioned optical thicknesses.

3.1.1. Cloud particle optical thickness. In situ measurements [*Esposito et al.*, 1983; *Ragent et al.*, 1985] showed that the cloud particle optical thickness at 365 nm is mostly between 25 and 35. We adopt 30 for b_p^c at 365 nm, and we verified that q calculated for this value of b_p^c differs mostly less than 0.005 from q calculated for b_p^c equal to 25 or 35. Values of b_p^c at other wavelengths were obtained by scaling the value at 365 nm according to the wavelength dependence of the cloud particle scattering coefficient, which was calculated using Mie theory.

We compared values of Venus' spherical albedo calculated according to our model for $b_p^c = 30$ with the observationally determined values of 0.87 and 0.90 at wavelengths of 550 nm and 935 nm, respectively. At these wavelengths, Venus' spherical albedo is essentially constant [cf. *Travis*, 1975; *Moroz*, 1983]. We found differences less than 0.01 between calculated and observed values.

3.1.2. Cloud molecular scattering optical thickness. We adopt 1.0 for b_{sm}^c at 365 nm, in agreement with the molecular scattering contribution derived by *Kawabata and Hansen* [1975] for a cloud-top pressure of 10 mbar. This value for the cloud molecular scattering optical thickness is slightly lower than the value of 1.35 deduced by *Hansen and Hovenier* [1974], and slightly higher than the value of 0.77 derived by *Kawabata et al.* [1980]. Values at other wavelengths are obtained by scaling with the wavelength dependent scattering coefficient of molecules. For our purposes, this dependence may be sufficiently approximated by the inverse fourth power of the wavelength.

3.1.3. Cloud molecular absorption optical thickness. Absorption is only taken into account at ultraviolet wavelengths, i.e., at 270 nm and 365 nm [cf. *Esposito et al.*, 1983]. The optical thicknesses of purely absorbing material at these wavelengths are indicated by $b_{am}^c(270)$ and $b_{am}^c(365)$, respectively. As shown by, e.g., *Travis* [1975], there is significant time variation of the spherical albedo of Venus at wavelengths shortward of 320 nm, but much less variation at wavelengths longward of 320 nm. Therefore we used $b_{am}^c(270)$ as a free parameter, and kept $b_{am}^c(365)$ fixed at 1.0. This value of the molecular absorption optical thickness at 365 nm results in a spherical albedo of Venus of approximately 0.5 at this wavelength, in agreement with values shown by *Travis* [1975]. At 270 nm, observed values of Venus' spherical albedo vary approximately between 0.25 and 0.6 [*Travis*, 1975]. According to calculations of Venus' spherical albedo with our model (see Figure 5), the observed values just mentioned correspond to values of $b_{am}^c(270)$ of about 5.5 and 0.5, respectively.

3.1.4. Haze particle optical thickness. The haze particle optical thickness, b_p^h, will be derived from

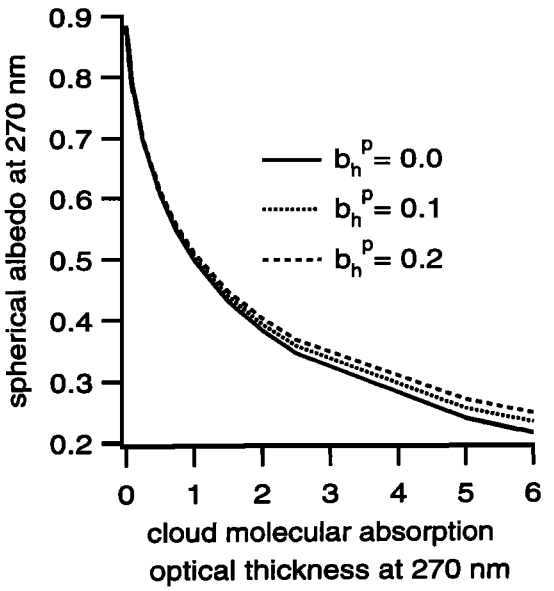

Figure 5. Venus' spherical albedo at 270 nm as a function of the cloud molecular absorption optical thickness for different values of the haze particle optical thickness b_p^h and for a cloud-top pressure of 2 mbar.

Pioneer Venus polarimetry data, as described further in this paper. From hereon, all values of b_p^h mentioned pertain to a wavelength of 365 nm. Values at other wavelengths were obtained by scaling according to the wavelength dependence of the scattering coefficient for haze particles, which was calculated using Mie theory.

3.1.5. Haze molecular scattering optical thickness. The optical thickness of scattering molecules above the cloud deck, b_{sm}^h, will also be derived from Pioneer Venus polarimetry data. This optical thickness is translated into a pressure level for the top of the cloud layer assuming a pure gaseous CO_2 atmosphere, using the relationship [cf. *Hansen and Travis*, 1974; *Kawabata et al.*, 1980]

$$\Pi_{ct} = \frac{6.17 \times 10^4 \lambda^4}{1 + 0.013\lambda^{-2}} b_{sm}^h, \quad (5)$$

where λ denotes the wavelength in microns and Π_{ct} denotes the pressure at the cloud-top in millibar. We note that this definition of cloud-top pressure is different from the definition used by *Hansen and Hovenier* [1974], who defined the cloud top pressure as the pressure corresponding to optical depth unity in the main cloud deck. Further in this work, we will employ Π_{ct} instead of b_{sm}^h.

Summarizing, the optical thicknesses due to the cloud particles, cloud molecular scattering, and cloud molecular absorption at 365 nm remain fixed in our analysis, whereas the optical thicknesses due to the haze particles, haze molecular scattering and cloud molecular absorption at 270 nm are used as free parameters. The influences of the changes in free parameter values on the phase angle dependence of the q component of the linear polarization are shown in the next section.

3.2. Cloud and Haze Particle Properties

Single scattering of light by haze and cloud particles is modeled by spheres having refractive indices corresponding to a concentrated sulfuric acid solution, as deduced by analysis of Earth-based polarimetry observations by *Hansen and Hovenier* [1974] for the cloud particles. The refractive indices deduced by *Kawabata et al.* [1980] and by *Sato et al.* [1996] for haze particles are in agreement with such a composition. Values for the four wavelengths at which polarization observations were made by the OCPP are 1.48, 1.46, 1.44, and 1.43, for 270, 365, 550, and 935 nm, respectively [cf. *Palmer and Williams*, 1975]. The single scattering albedos of cloud and haze particles equal unity.

The cloud and haze particles are distributed in size according to a gamma distribution, which is characterized by an effective radius r_{eff} and an effective variance v_{eff} [cf. *Hansen and Travis*, 1974; *Hansen and Hovenier*, 1974]. Values for the cloud and haze particles will be denoted by superscripts c and h, respectively. For the cloud particles, we adopted values derived by *Hansen and Hovenier* [1974], i.e., $r_{eff}^c = 1.05$ μm and $v_{eff}^c = 0.07$. For the haze particles, we adopted $r_{eff}^h = 0.25$ μm and $v_{eff}^h = 0.17$ after *Kawabata et al.* [1980]. These size distributions are consistent with recent results obtained by *Sato et al.* [1996] and *Knibbe et al.* [1997].

Single scattering properties of cloud and haze particles were calculated using Mie theory and expressed in coefficients for expansions in generalized spherical functions [cf. *De Rooij and van der Stap*, 1984]. These coefficients have been used in our adding/doubling code. Figure 6 displays single scattering results of q for cloud and haze particles, for the four wavelengths that we consider. Apart from strong wavelength dependences, it shows that large differences occur between values of q as calculated for cloud and haze particles.

4. Theoretical Phase Angle Dependence of Linear Polarization

The phase angle dependence of the polarization of Venus has appeared to be very informative of Venus' atmospheric structure and composition. We show in this section theoretical results of the phase angle dependence of q, which may be compared to the Pioneer Venus observations shown in Figure 2. Such a comparison indicates that time variations of the polarization as observed by the Pioneer Venus Orbiter may be caused by variations in the free parameters presented in the previous section. Moreover, these theoretical results indicate that q near a phase angle of 90° is quite sensitive to changes in free parameter values. All theoretical results shown in this section have been calculated for a typical distance of 60,000 km between the orbiter and the planetary surface. No results are shown for phase

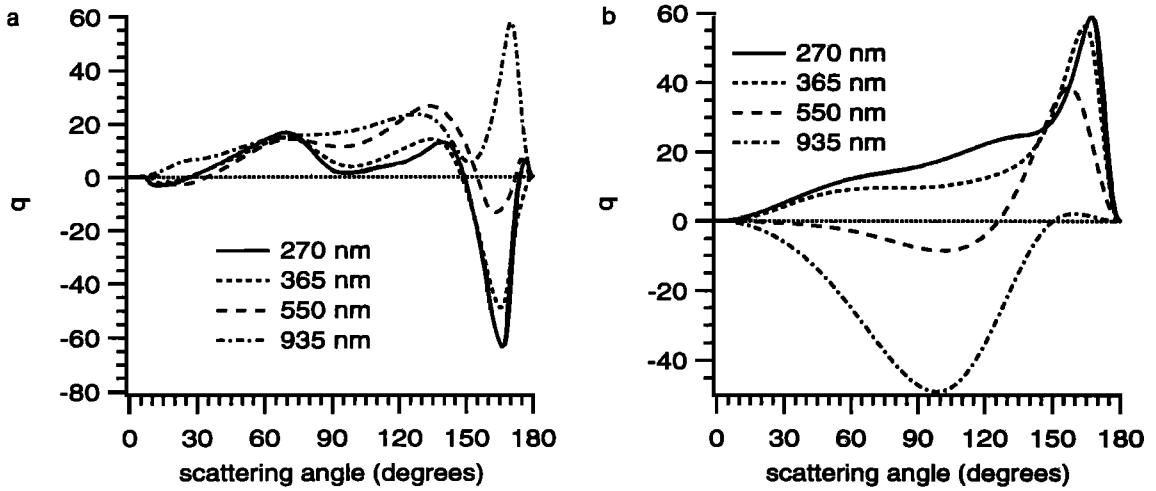

Figure 6. Simulated values of q in percent as functions of scattering angle calculated for single scattering by an ensemble of (a) cloud particles and (b) haze particles, for the four wavelengths considered. Here the incident light is unpolarized.

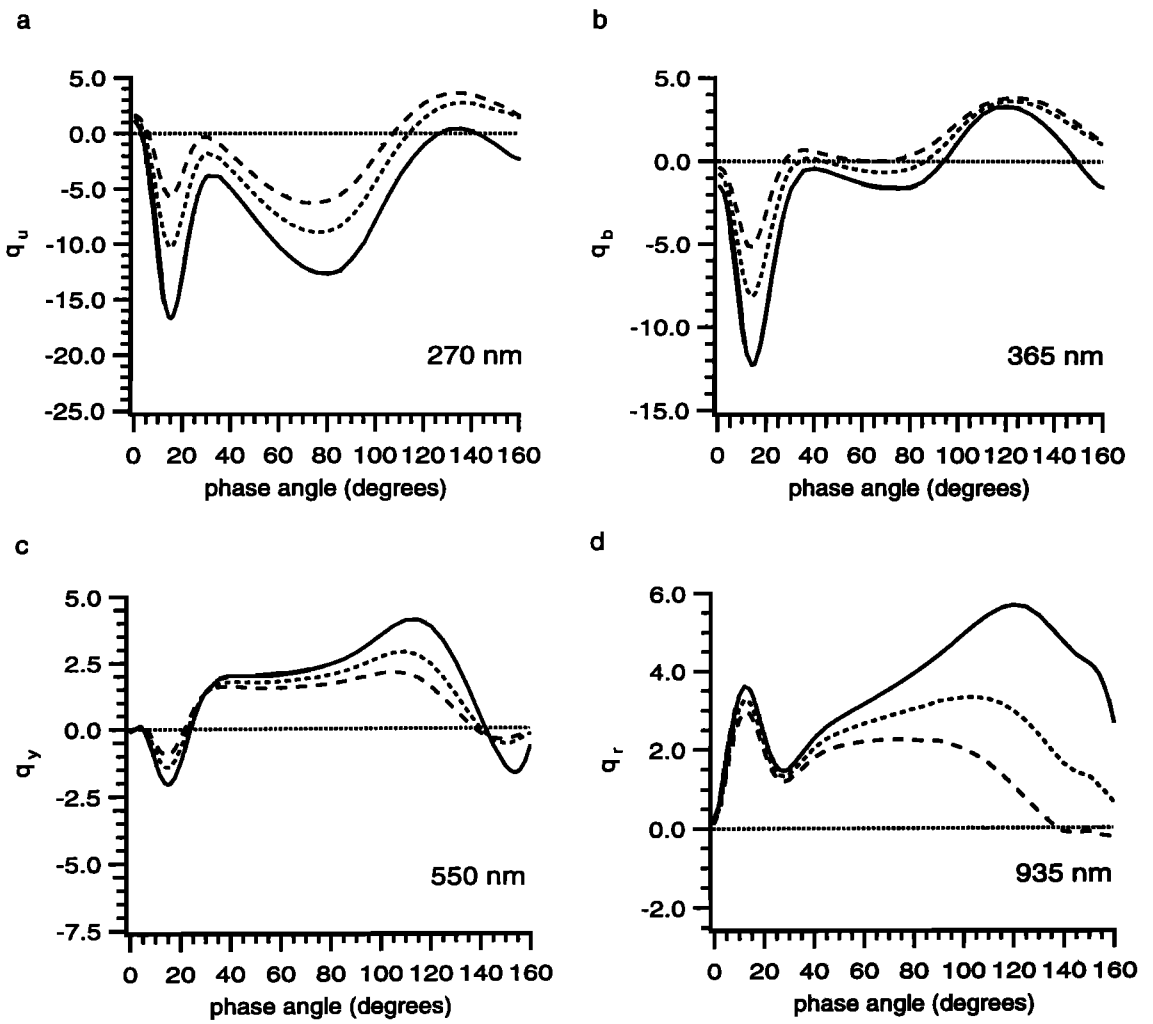

Figure 7. Simulated values of q in percent as a function of the phase angle, for different values of the haze particle optical thickness b_p^h and four wavelengths. Here the cloud molecular absorption optical thickness at 270 nm is 2.0, and the cloud-top pressure is 2 mbar. The solid, dotted, and dashed curves indicate values calculated for $b_p^h = 0.0$, 0.1, and 0.2, respectively.

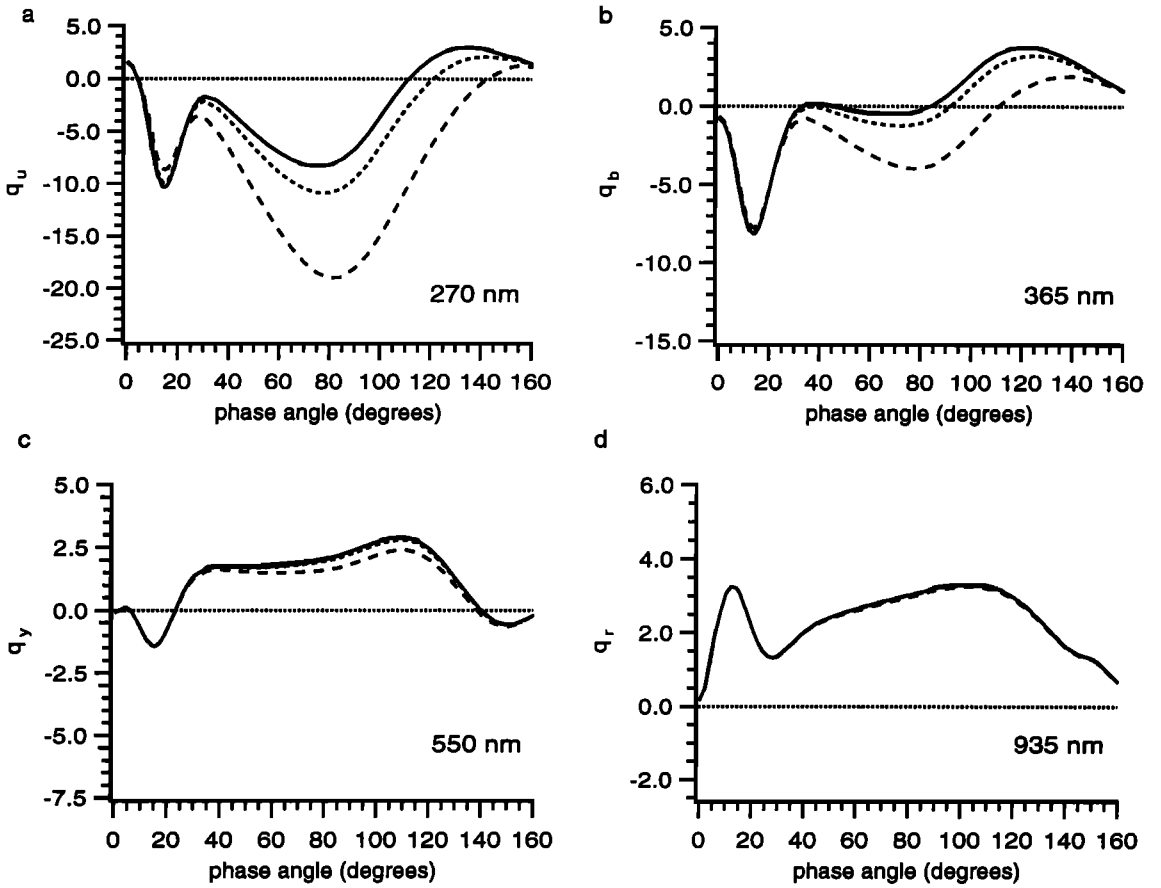

Figure 8. Simulated values of q in percent as a function of the phase angle, for different values of the cloud-top pressure Π_{ct} and four wavelengths. Here the cloud molecular absorption optical thickness at 270 nm is 2.0 and the haze particle optical thickness is 0.1. The solid, dotted, and dashed curves indicate values calculated for Π_{ct} = 1, 5, and 20 mbar, respectively.

angles larger than 160°, since all observations pertain to phase angles less than 160°.

Figure 7 shows theoretical results of q as functions of phase angle for different values of b_p^h, for the four wavelengths considered. These results pertain to calculations for which we adopted $b_{am}^c(270) = 2.0$ and $\Pi_{ct} = 2$ mbar. At 270 nm, increasing the haze optical thickness from 0.0 to 0.2 increases q_u for all phase angles shown in Figure 7a. Comparison of these theoretical results with the observations displayed in Figure 2a indicates that, apparently, a value of b_p^h of 0.2 leads to values of q_u that correspond closely to the values observed in 1979 for most phase angles. It is also seen that theoretical results of q_u for $b_p^h = 0.0$ correspond more closely to the values observed in 1981 and 1989.

Considering the theoretical results at 365 nm of Figure 7b, an increase of b_p^h from 0.0 to 0.2 also increases q_b for all phase angles, but here the increase is generally smaller than that of q_u. Comparing these theoretical results with the observed values in Figure 2b, it appears that also for 365 nm the observed values of 1979 correspond more closely to theoretical results for b_p^h 0.2, whereas the observed values of 1981 and 1989 correspond more closely to theoretical results for $b_p^h = 0.0$.

At 550 nm, increasing b_p^h from 0.0 to 0.2 brings q_y closer to zero, except for phase angles between approximately 20° and 30°, and near 150°. It is shown in Figure 2c that the values of q_y observed in 1979 tend to be closer to zero than those observed in 1981 and 1989. Thus observations of q_y made in 1979 correspond more closely to theoretical values of q_b calculated for $b_p^h = 0.2$, whereas observations of q_y made in 1981 and 1989 correspond more closely to theoretical results for $b_p^h = 0.0$.

Values of q_r displayed in Figure 7d decrease for all phase angles shown when b_p^h increases from 0.0 to 0.2. Comparing these results with the obervations of Figure 2d, apparently, observations made in 1979 correspond to a larger haze optical thickness than observations made in 1981 and 1989.

Summarizing, the sensitivity of q to changes of b_p^h is, at the four wavelengths considered, large for phase angles near 90°. Further, this sensitivity mostly increases with decreasing phase angle for q_u and q_b, but mostly decreases with decreasing phase angle for q_y and q_r.

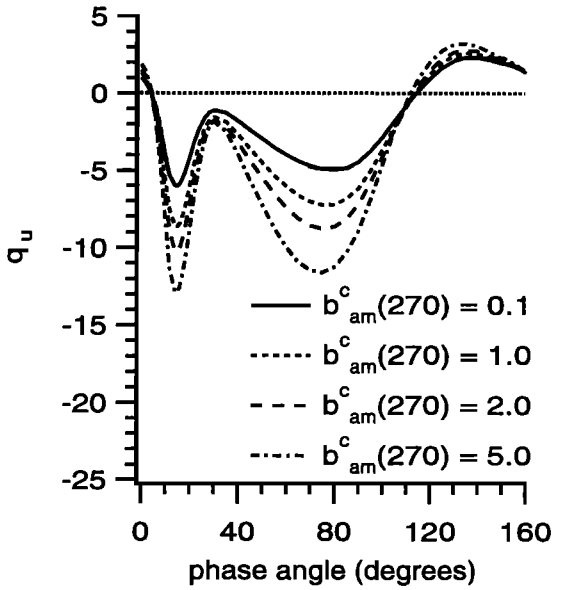

Figure 9. Simulated values of q_u in percent as a function of the phase angle, for different values of the cloud molecular absorption optical thickness $b^c_{am}(270)$. Here the cloud-top pressure is 2 mbar and the haze particle optical thickness is 0.1.

Therefore we have chosen to use the phase angle interval between 80° and 100° to investigate changes of b^h_p.

Figure 8 shows the influence of Π_{ct} on the phase angle dependence of q for the four wavelengths considered. The results shown in this figure pertain to calculations for which we adopted $b^h_p = 0.1$ and $b^c_{am}(270) = 2.0$. The influence of Π_{ct} on q evidently decreases with increasing wavelength. For instance, whereas a difference of 19 mbar in Π_{ct} corresponds to a difference in q_u at a phase angle of 100° of about 11%, it corresponds to differences in q_b, q_y, and q_r at the same phase angle of about 3.5%, 0.5% and 0.1%, respectively. For 270 nm, this difference remains approximately 11% for phase angles between 80° and 100°, and is mostly smaller for other phase angles. Also at 365 nm and 500 nm, the sensitivity of q to changes of Π_{ct} is largest at these phase angles.

We further note that, when assuming that $b^h_p = 0.1$ is an average value for the haze optical thickness, theoretical results for q at all four wavelengths, calculated for 1 mbar $\leq \Pi_{ct} \leq$ 20 mbar, are in reasonable agreement with the observations shown in Figure 2.

Figure 9 shows the influence of $b^c_{am}(270)$ on the phase angle dependence of q_u, calculated for $\Pi_{ct} = 2$ mbar and $b^h_p = 0.1$. It appears that increasing $b^c_{am}(270)$ increases the absolute value of q_u at all phase angles, except near phase angles where $q_u = 0.0$. Comparing these theoretical results with observations of q_u displayed in Figure 2a, it follows that q_u, as calculated for values of $b^c_{am}(270)$ in the range between 0.5 and 5.0, agrees reasonably well with observed results. This is consistent with the theoretical behavior of Venus' spherical albedo, as discussed in section 3.

5. Determining Free Parameters With Newton-Raphson Iteration

In the previous section, theoretical results were compared with observed values. From such a direct comparison it is difficult to determine free parameter values precisely. Therefore, we present in this section a more advanced approach for deducing free parameter values from the observations. This approach employs theoretical calculations in an iterative procedure for solving a set of equations.

The concept of iteratively solving systems of nonlinear equations using first derivatives of the functions involved is well known, and is usually called Newton–Raphson iteration [cf. *Press et al.*, 1992, chap. 9; *Stoer and Bulirsch* 1993, chap. 5; *Hildebrand* 1974, chap. 10]. This procedure may be applied to the interpretation of satellite polarimetry data by formally writing this interpretation in terms of nonlinear equations. These equations will be presented later in this section. Application of this approach has several advantages. For instance, there is no need to perform a large number of theoretical calculations in advance, such as would be needed for analyses based on lookup tables. On the contrary, given a first guess of the atmosphere properties to be derived, theoretical calculations are steered in order to reduce differences between observed and theoretical polarization, and terminated when the agreement is judged sufficient. Further, this approach allows combining observations at different wavelengths and deriving several atmosphere properties simultaneously. Because Newton–Raphson iteration does not always produce acceptable solutions [cf. *Press et al.*, 1992, chap. 9], we present in this section a number of tests of our implementation. In addition, we estimate the influence of measurement errors of q on the derived values of atmosphere properties.

Using the superscript 'm' for values measured by the Pioneer Venus Orbiter, the following equations were employed:

$$q^m_u - q_u(b^h_p, \Pi_{ct}, b^c_{am}(270)) = 0, \quad (6)$$

$$q^m_b - q_b(b^h_p, \Pi_{ct}) = 0, \quad (7)$$

$$q^m_y - q_y(b^h_p, \Pi_{ct}) = 0, \quad (8)$$

$$q^m_r - q_r(b^h_p, \Pi_{ct}) = 0. \quad (9)$$

The theoretical values, which depend on the haze optical thickness b^h_p, cloud-top pressure Π_{ct}, and for 270 nm also on the molecular absorption optical thickness within the clouds $b^c_{am}(270)$, are still indicated by q without a superscript. The dependence of q on other model parameters, which have fixed values in our analysis, is not indicated in Eqs. (6) – (9).

Different combinations of these equations were employed in order to derive free parameter values. These combinations were labeled by the same letters as used for q at the four wavelength observed, as follows. We will use the letters U, B, Y, and R for Eqs. (6) – (9),

respectively. The combinations of Eqs. (7) and (8), denoted by BY, and Eqs. (7) and (9), denoted by BR, were used in order to derive b_p^h and Π_{ct}. The redundancy of three equations to deduce two unknowns was employed to investigate the consistency of the values derived from combinations BY and BR. The combinations of Eqs. (6), (7), and (8), indicated by UBY, and of Eqs. (6), (7), and (9), indicated by UBR, were used to deduce $b_{am}^c(270)$, b_p^h and Π_{ct}. Here, the redundancy of four equations to determine three unknowns is also used to investigate the consistency of the values derived from combinations UBY and UBR.

The iterative Newton–Raphson method was employed to find the zeros of Eqs. (6) – (9), since these zeros correspond to theoretical values of q which are equal to the observed values. As elaborated by *Press et al.* [1992, chap. 9], it is very important to have information about the behaviour of the nonlinear equations, and to be able to provide a good first guess of the free parameters when using the method of Newton–Raphson. The reason is that only local convergence of this method is good, whereas convergence over large regions in the parameter space may well be poor. Considering the behavior of the equations, we investigated the theoretical dependence of q_u, q_b, q_y, and q_r on the free parameters for phase angles near 90°. We found that the dependence of q at all four wavelengths on b_p^h, Π_{ct}, and $b_{am}^c(270)$ is smooth. Therefore, it is unlikely that pathological cases, as mentioned by *Press et al.* [1992, chap. 9], will occur. Regarding a first guess, it was shown in section 4 that theoretical values of q corresponding to $0.0 \leq b_p^h \leq 0.2$, 1 mbar $\leq \Pi_{ct} \leq$ 20 mbar, and $0.1 \leq b_{am}^c(270) \leq 5.0$ agree reasonably well with most observed values of q, so that values for the free parameters in these ranges may indeed serve as first guesses. We adopted $b_p^h = 0.1$, $\Pi_{ct} = 1$ mbar, and $b_{am}^c(270) = 2.0$ for this purpose.

The partial derivatives of q to the free parameters, which are needed in the Newton–Raphson method, have been evaluated numerically, because no simple analytical expression is available for this purpose. We used a forward–difference approximation, analogous to the method mentioned by *Press et al.* [1992, chap. 9]. This approximation may be written in one dimension as

$$\frac{df(x)}{dx} \simeq \frac{f(x+dx) - f(x)}{dx}, \tag{10}$$

where x denotes a free parameter (i.e., one of b_p^h, Π_{ct}, and $b_{am}^c(270)$), dx the corresponding difference, and $f(x)$ the function to be differentiated (i.e., one of q_u, q_b, q_y, and q_r). However, we used fixed differences for b_p^h, Π_{ct}, and $b_{am}^c(270)$, equal to 0.05, 0.5, and 0.1, respectively, whereas the method mentioned by *Press et al.* [1992, chap. 9] uses variable differences. Tests using other values of these differences did not significantly alter our results. We stopped the iterations when the derived values differed less than these fixed differences from the free parameter values at which the derivatives were last calculated. This condition may be written in one dimension as

$$|x_{derived} - x| < dx, \tag{11}$$

where $x_{derived}$ and x denote the derived value of x and the value at which the derivative of $f(x)$ was last determined, respectively.

Tests of this method were performed in the following way. Theoretical values of q_u, q_b, q_y, and q_r were calculated for certain values of b_p^h, Π_{ct}, and $b_{am}^c(270)$. These theoretical values were then treated as (simulated) observational results. So, they were substituted for q_u^m, q_b^m, q_y^m, and q_r^m in Eqs. (6) – (9) and the Newton–Raphson iteration was started in order to determine free parameter values from these simulated observations. The derived values should correspond to the known values used to calculate the simulated observations. Tables 1 and 2 display derived free parameter values obtained in this manner from observations simulated for the typical values of $b_p^h = 0.17$, $\Pi_{ct} = 11$ mbar, and $b_{am}^c(270) = 1.5$. In addition, these tables show the influence of measurement errors in q on derived parameter values. The results in these tables were obtained for observations made at a disk–centered phase angle of 90°, at a distance of 60,000 km from the planetary surface. By performing additional calculations for different phase angles and distances, we found that the results listed in Tables 1 and 2 are typical for the phase angles and distances considered in this paper.

The upper part of Table 1 reports values of b_p^h and Π_{ct} derived using combinations BY and BR. Apparently, the desired solutions are found after a few iterations. The lower part of Table 1 shows b_p^h and Π_{ct} as obtained from simulated observations with simulated errors. For the

Table 1. Test Results of Newton–Raphson Solution of Combinations BY and BR, Obtained From Observations Simulated for $b_p^h = 0.17$ and $\Pi_{ct} = 11$ mbar

Iteration	BY	BR
1	0.16998 / 9.71	0.16902 / 9.67
2	0.16853 / 10.84	0.16895 / 10.86
3	0.16865 / 10.95	0.16898 / 10.97
Error	**BY**	**BR**
+0.002	0.13822 / 8.16	0.15087 / 8.83
−0.002	0.19904 / 14.19	0.18695 / 13.34
+0.0002	0.16567 / 10.73	0.16715 / 10.82
−0.0002	0.17173 / 11.28	0.17078 / 11.23

The iterations were started at $b_p^h = 0.1$ and $\Pi_{ct} = 1$ mbar. The upper part of this table shows results obtained after successive iterations. The lower part displays results obtained from simulated observations with simulated measurement errors. The second and third columns of the entire table show derived values of b_p^h / Π_{ct} (in mbar), obtained from the pertinent wavelength combinations.

Table 2. Test Results of Newton–Raphson Solution of $b^{c}_{am}(270)$ for Combinations UBY and UBR, Obtained From Observations Simulated for $b^{h}_{p} = 0.17$, $\Pi_{ct} = 11$ mbar, and $b^{c}_{am}(270) = 1.5$

Iteration	UBY	UBR
1	0.56246	0.55592
2	1.18635	1.18697
3	1.38022	1.38094
4	1.43891	1.43976
5	1.46406	1.46490

Error		UBY	UBR
270 nm	Other		
+0.01	+0.002	1.12055	1.14650
−0.01	−0.002	1.84595	1.82629
+0.001	+0.0002	1.44697	1.45092
−0.001	−0.0002	1.51306	1.51048

The iterations were started at $b^{h}_{p} = 0.1$, $\Pi_{ct} = 1$ mbar, and $b^{c}_{am}(270) = 2.0$. The upper part of this table shows results obtained after successive iterations. The lower part displays results obtained for different simulated measurement errors. The results for b^{h}_{p} and Π_{ct} virtually coincide with those given in Table 1, and are not shown here.

measurement errors, we used 0.002 and 0.0002. Here, 0.002 corresponds to the measurement errors in q^{m}_{b}, q^{m}_{y}, and q^{m}_{r} pertaining to individual pixels, whereas 0.0002 represents measurement errors pertaining to disk averages of q^{m}_{b}, q^{m}_{y}, and q^{m}_{r}, as discussed in section 2. Whereas errors of 0.002 in q may cause b^{h}_{p} to differ at most 0.04 from the actual value, errors in q of 0.0002 induce errors in b^{h}_{p} of less than 0.01. The errors in the derived values of Π_{ct} are at most about 3 mbar and 1 mbar for errors in q of 0.002 and 0.0002, respectively.

The upper part of Table 2 lists derived values of $b^{c}_{am}(270)$ after successive iterations, which were obtained by using combinations UBY and UBR. The corresponding derived values of b^{h}_{p} and Π_{ct} are not listed in Table 2, since they virtually coincide with those listed in Table 1. This means that b^{h}_{p} and Π_{ct} are determined by either the combination BY or BR. Adding equation (6) to these combinations with $b^{c}_{am}(270)$ as a free paremeter does not change the derived values of b^{h}_{p} or Π_{ct}, but in addition, a value for $b^{c}_{am}(270)$ is derived which is consistent with b^{h}_{p} and Π_{ct}. This apparently requires, however, more iterations than are needed when only b^{h}_{p} and Π_{ct} are derived. This is probably caused by the low values of $b^{c}_{am}(270)$ obtained in the first iteration. We note that these low values are further away from the correct value of 1.5 than the first guess of 2.0. In tests for different model specifications, it was found that including (6) led to similar increases in the number of required iterations.

The lower part of Table 2 lists derived values of $b^{c}_{am}(270)$ as obtained from simulated observations with simulated errors. Here, errors in the simulated values of q_{u} were used of 0.01 and 0.001, when the errors in the simulated values of q_{b}, q_{y}, and q_{r} equalled 0.002 and 0.0002, respectively. Apparently, errors induced in the derived values of $b^{c}_{am}(270)$ by errors in q_{u} of 0.01 and 0.001 are at most about 0.35 and 0.05, respectively.

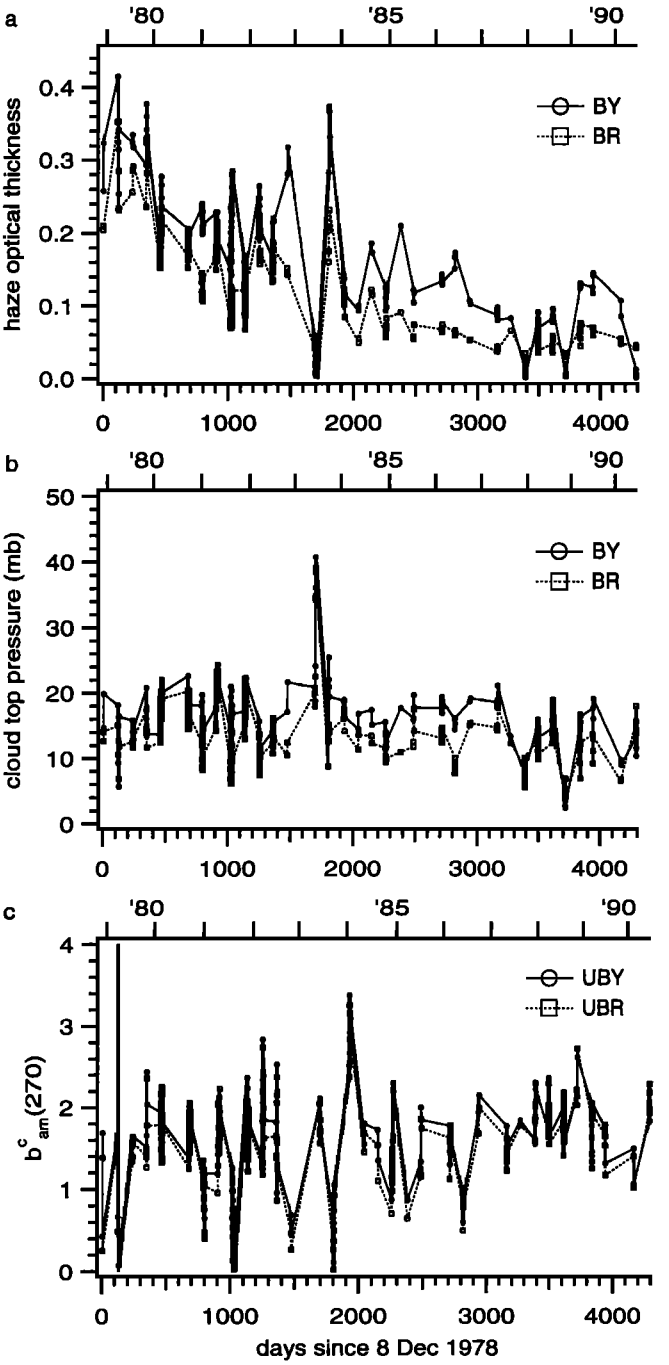

Figure 10. (a) Haze optical thickness, (b) cloud-top pressure, (c) and cloud molecular absorption optical thickness at 270 nm $b^{c}_{am}(270)$ as a function of time. These values were derived from the observations displayed in Figure 3, using combinations BY and BR for the haze particle optical thickness and cloud-top pressure, and combinations UBY and UBR for $b^{c}_{am}(270)$.

We conclude from these tests that, using simulated data, our procedure enables us to retrieve free parameter values with high accuracy. Therefore application of our procedure to Pioneer Venus data will expectedly provide reliable results.

6. Interpretation of Observations

The method described in the previous section has been applied to the 267 selected maps to derive haze optical thickness and cloud-top pressure, using combinations BY and BR, and to deduce the molecular absorption optical thickness at 270 nm, using combinations UBY and UBR. The resulting values of b_p^h, Π_{ct}, and $b_{am}^c(270)$ are shown in Figure 10 as functions of time. We note that, as shown in Tables 1 and 2, inaccuracies in the derived values of b_p^h, Π_{ct}, and $b_{am}^c(270)$ due to measurement errors are at most about 0.04, 3 mbar, and 0.35, respectively.

Figure 10a shows values of b_p^h that are of the order of 0.25 in 1978 and of the order of 0.1 or smaller in 1990. Although the derived values of b_p^h are apparently lower after approximately day 2000 than before this day, there are significant short-term variations. These variations are larger than the maximum inaccuracies of 0.04 in derived values of b_p^h caused by measurement errors. For instance, near day 1000, b_p^h increases from less than 0.1 to more than 0.2 in a relatively short time. Near day 1700, which is in the year 1983, the derived values of b_p^h are close to zero. In fact, a few values (not shown) lie even a few hundredths below zero. However, large values of b_p^h of the order of 0.2 and 0.4 pertaining to values derived using combination BY and BR, respectively, are found less than 200 days later. It can also be seen in Figure 10a that values of b_p^h derived from combinations BY and BR usually differ by less than 0.1, but may exceptionally differ by 0.2, such as near days 1500 and 1800.

The derived values of cloud-top pressure, shown in Figure 10b, remain mostly of the order of 15 mbar during the entire period from 1978 to 1990, with irregular variations generally between 5 and 20 mbar. Exceptional behavior occurs near day 1700, where Π_{ct} suddenly reaches values as high as 40 mbar. These exceptionally high values coincide with the low values of b_p^h near day 1700. Cloud-top pressures derived from combination BY are generally somewhat lower than those obtained from combination BR.

The differences between the values of b_p^h and Π_{ct} as derived from combinations BY and BR were investigated more closely, for a sample of the 267 selected maps. This selection consists of maps made at days 7, 1475, 1806, 2382, 3611, 3837 and 3840. At these days, rather high differences were found, as shown in Figures 10a and 10b. Properties of the haze layer were varied, and we found that these differences became smaller when using a somewhat smaller value for r_{eff}^h than 0.25 μm to interpret these observations. To exemplify this, Table 3 displays values of b_p^h and Π_{ct} derived for $r_{eff}^h = 0.20$ μm compared with those derived for $r_{eff}^h = 0.25$ μm. Apparently, b_p^h and Π_{ct} deduced from combination BY are more sensitive to this change in r_{eff}^h than those obtained from combination BR. We conclude that at these dates the haze particles are probably somewhat smaller than 0.25 μm. A value of 0.20 μm for r_{eff}^h is still in agreement with haze particle size distributions reported by *Sato et al.* [1996] and *Knibbe et al.* [1997].

Table 3. Comparison of Values of Haze Optical Thickness and Cloud-Top Pressure Derived for $r_{eff}^h = 0.25$ μm and $r_{eff}^h = 0.20$ μm, With Combinations BY and BR

Day	BY (0.25)	BY (0.20)	BR (0.25)	BR (0.20)
	Haze Optical Thickness			
7	0.26	0.19	0.21	0.19
1475	0.32	0.19	0.14	0.13
1806	0.37	0.22	0.21	0.19
2382	0.21	0.13	0.09	0.09
3611	0.08	0.06	0.05	0.05
3837	0.13	0.09	0.04	0.05
3840	0.13	0.09	0.08	0.07
	Cloud-Top Pressure, mbar			
7	15	8	13	8
1475	22	10	12	9
1806	22	9	14	8
2382	18	10	11	9
3611	18	15	16	15
3837	13	10	7	8
3840	15	11	12	10

"Day" column displays the day of observation, since the start at December 8, 1978.

Using $r_{eff}^h = 0.20$ μm instead of $r_{eff}^h = 0.25$ μm, b_p^h and Π_{ct} were derived from a larger selection of maps than used for Table 3. It was found that, generally, differences between the results derived with $r_{eff}^h = 0.20$ μm and 0.25 μm are similar to differences seen in Table 3. In particular, the results displayed in Figures 10a and 10b for combination BR are not very different from results derived using $r_{eff}^h = 0.20$ μm instead of $r_{eff}^h = 0.25$ μm. Therefore a similar time evolution of b_p^h and Π_{ct} is derived with $r_{eff}^h = 0.20$ μm as with $r_{eff}^h = 0.25$ μm.

The derived values of $b_{am}^c(270)$ displayed in Figure 10c show significant time variations, around a mean value of about 1.5. Most values lie between 0.5 and 4.0. However, near day 125, a few exceptionally high values were derived, which are off-scale. From combinations UBY and UBR, namely, on day 123 (April 9, 1979), values of 4.4 and 4.8 were derived, respectively, and on day 127 (April 13, 1979), values of 9.7 and 22.7, respectively.

On the other hand, some values lower than 0.5 were also deduced.

The very low values of b_p^h and very high values of cloud-top pressure found near day 1700 correspond to rather low values of $b_{am}^c(270)$. However, similarly low values of $b_{am}^c(270)$ are derived near day 1000, so that the behavior of $b_{am}^c(270)$ near day 1700 does not appear as exceptional as that of b_p^h and Π_{ct}. The rather high values of $b_{am}^c(270)$ of about 3.4 deduced near day 1900 do not correspond to a special behavior of b_p^h or Π_{ct}, as can be seen in Figure 10. So there does not seem to be a strong correlation between the absorption optical thickness at 270 nm and anomalous behavior of cloud-top pressure or haze optical thickness.

The influence on derived values of $b_{am}^c(270)$ of changing $r_{eff}^h = 0.25$ μm to 0.20 μm was investigated. Derived values appeared in general to change less than 0.5, but differences between results derived from combinations UBY and UBR increased. These differences increased to about 1.0, whereas they are smaller when using $r_{eff}^h = 0.25$ μm, as can be seen in Figure 10c. Therefore we conclude that $r_{eff}^h = 0.20$ μm is not more consistent with the observations at all four wavelengths than $r_{eff}^h = 0.25$ μm.

The exceptionally high values of Π_{ct} and low values of b_p^h found near day 1700 correspond to observations made in 1983 during the period of half a Venusian sidereal year, which are displayed in Figure 2. Our results agree with the suggestion by *Sato et al.* [1996] of the absence of haze particles and high cloud-top pressures during the same period for the polar regions. A number of the observations made in 1983 at phase angles outside the range from 80° to 100°, however, differ significantly from theoretical calculations for free parameter values within the ranges that we expect, as can be seen by comparing Figure 2 with Figures 7 – 9. Therefore more extensive research than presented in this paper will be necessary to explain the observations made in 1983.

In order to quantify the correlation between the derived time variations of b_p^h, Π_{ct}, and $b_{am}^c(270)$, we calculated the coefficients of linear correlation [cf. *Draper and Smith*, 1966] for these time variations. The resulting values shown in Table 4 indicate that the correlations are small.

Table 4. Coefficients of Linear Correlation Between Time Variations of b_p^h, Π_{ct}, and $b_{am}^c(270)$

Correlation Between	(U)BY	(U)BR
b_p^h and Π_{ct}	0.18	0.21
b_p^h and $b_{am}^c(270)$	–0.21	0.16
Π_{ct} and $b_{am}^c(270)$	–0.13	0.06

Time variations of b_p^h and Π_{ct} were derived from wavelength combinations BY and BR, time variations of $b_{am}^c(270)$ were derived from wavelength combinations UBY and UBR.

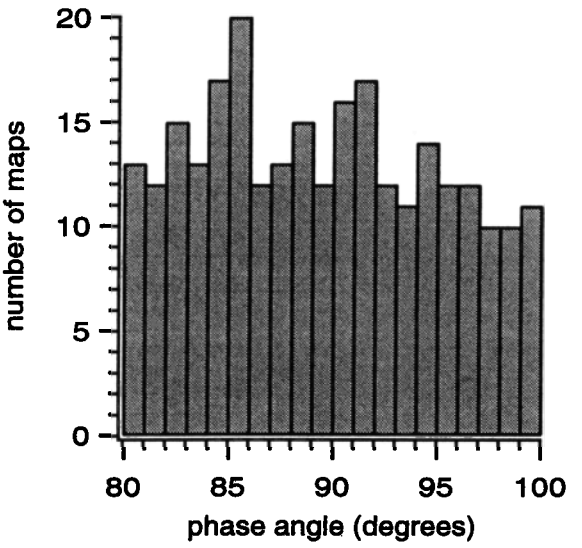

Figure 11. Histogram of the phase angles of the selected maps.

The evolutions of b_p^h, Π_{ct}, and $b_{am}^c(270)$ shown in Figure 10 were derived from 267 maps made at disk-centered phase angles from 80° to 100°, out of a total of about 2000 maps. As can be seen in Figure 1, there are fewer observations after day 2500 with phase angles in the high end of our interval from 80° to 100° than before day 2500. Therefore we investigated if the derived values of the free parameters, and especially the apparently lower values of b_p^h derived after day 2000, are correlated to the phase angle. Such a correlation might introduce a bias in the results pertaining to the period after day 2500. However, we found no correlation between derived values of either b_p^h, Π_{ct}, or $b_{am}^c(270)$ and the disk-centered phase angle. For this reason, we do not expect that the more limited phase angle range of the observations made after day 2500 introduces a bias in our results.

It was also checked if uneven sampling of phase angles or time may have influenced the derived free parameter values. For that purpose, we determined the distributions of our selection of maps over phase angle and time. The distribution over phase angles is shown in Figure 11. In this figure, the numbers of maps having disk-centered phase angles in bins of 1° width are displayed. The selection used in the analysis presented in this paper appears to be rather evenly distributed over the phase angle range between 80° and 100°.

The distribution of the selected maps over time is shown in Figure 12. This figure displays the numbers of maps which were obtained in bins having widths of approximately half a Venusian sidereal year. Evidently, many observations were obtained between days 400 and 1200. Interestingly, the numbers of observations selected during periods of half a Venusian sidereal year from day 2500 onward, are not much lower than between days 0 and 400, and between days 1200 and 2500, al-

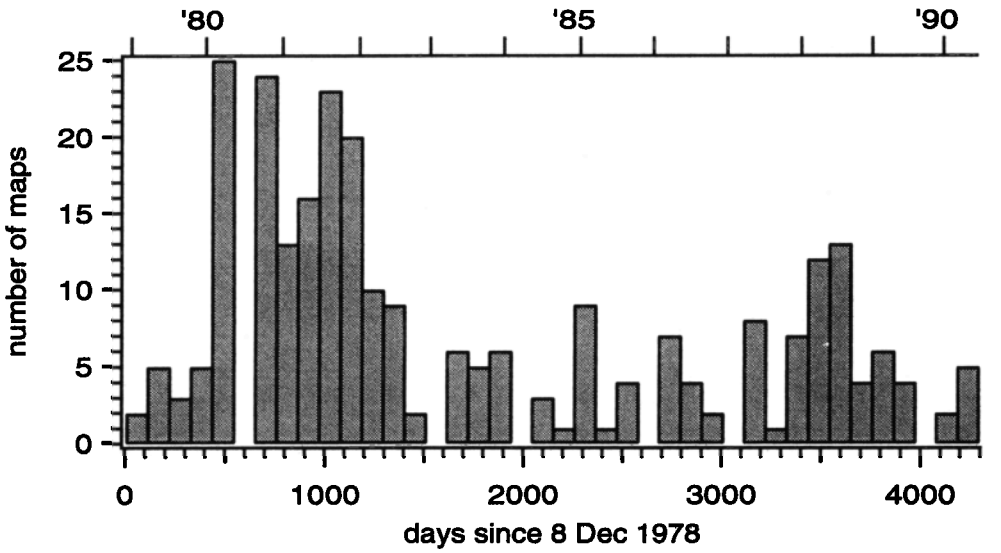

Figure 12. Histogram of the days of the selected maps.

though the phase angle range of the observations made after day 2500 is more limited.

The distributions shown in Figures 11 and 12 indicate a rather even distribution of our selection over phase angles between 80° and 100°, and also that a significant number of maps was obtained after day 2500. Since we also found no correlation of our results with phase angles, it seems probable that the derived free parameter values have not been influenced by selection effects and, in particular, that the generally lower values of b_p^h derived for days later than approximately day 2000 correspond to actually lower haze optical thicknesses on Venus.

In order to determine if a long-term trend in haze optical thickness occurred, we first determined sliding averages of b_p^h over periods having a length of four Venusian sidereal years. In this way, the derived short-term variations are smoothed. These averages, calculated every quarter of a Venusian sidereal year, are displayed in Figure 13. In this figure, it appears that both these averages clearly indicate that the haze optical thickness decreased during the Pioneer Venus mission. We note that the values of b_p^h derived from combination BR may be considered as more significant, since these are less sensitive to small changes in r_{eff}^h than those derived from combination BY.

Next, we estimated the magnitude of the trend in b_p^h. For this purpose, we assumed a linear decrease of b_p^h with time. The usage of linear approximations for characterizing climatic variability is discussed by, e.g., *Polyak* [1996]. Descriptions of linear regression and the use of the t–statistic to determine confidence intervals may be found in various statistical textbooks, such as *Draper and Smith* [1966] and *Gunst and Mason* [1980]. Concerning the magnitude of the trend, we found, using linear regression, average decreases in b_p^h of 1.2×10^{-2} and 1.1×10^{-2} per Venusian sidereal year, for the combinations BY and BR, respectively. The 95% confidence intervals centered on these average decreases both have a width of 0.2×10^{-2}.

As a last check of our results, we investigated briefly if the free parameter values derived from observations made between phase angles of 80° and 100° are consistent with observations made at other phase angles. For that purpose, we compared values of q observed at phase angles close to 15°, 60°, and 150° with theoretical results. It was found that, in general, the observed values agree with theoretical results for average values

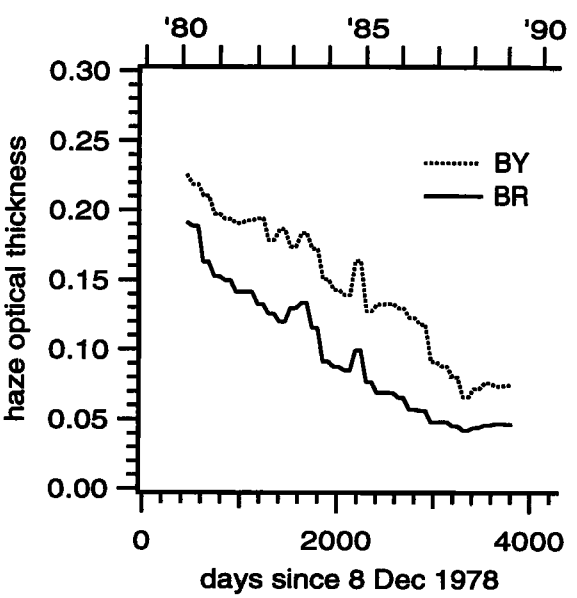

Figure 13. Sliding averages of haze optical thickness as a function of time. The averages of the derived values were calculated over periods of four Venusian sidereal years, every quarter of a Venusian sidereal year. They are displayed at the days corresponding to centers of these periods. The averages are connected by straight lines.

of 15 mbar for Π_{ct}, 1.5 for $b^c_{am}(270)$, and about 0.1 for b^h_p. Moreover, most of these observations also indicate a decreasing haze optical thickness. Only a small number of values of q_y observed near a phase angle of 15° agreed with values of b^h_p of the order of 0.2, whereas simultaneous observations of q_u, q_b, and q_y were consistent with lower values of b^h_p, namely, of 0.1 or less.

7. Discussion and Conclusions

In our analysis of Pioneer Venus polarimetry data, we employed a model atmosphere consisting of a cloud and a haze layer. This model is based on earlier research of Venus' atmosphere. We assumed that all model parameters remained constant during the Pioneer Venus mission, except three free parameters, namely the haze optical thickness, cloud-top pressure, and cloud absorption optical thickness at 270 nm.

We employed Newton–Raphson iteration for the interpretation of a selection of disk–averaged Pioneer Venus polarization observations, as an initial attempt to chart long term variations of disk–averaged atmosphere properties from these observations. Using this method, and observations at all four wavelengths, we have simultaneously derived values for the free parameters. The selected observations cover the entire period in which polarization data were obtained by the Pioneer Venus orbiter, and were made at phase angles between 80° and 100°.

Newton–Raphson iteration was tested using simulated observations, demonstrating that the procedure gives accurate results. In addition, a sensitivity analysis showed that errors in derived values of b^h_p, Π_{ct} and $b^c_{am}(270)$ induced by measurement errors are at most about 0.04, 3 mbar, and 0.35, respectively. Thus Newton–Raphson iteration is an excellent method to derive atmospheric model parameters from spectral polarization data.

In principle, the method described and employed in this work may well be applied to a different selection of Pioneer Venus polarization observations. Then, for instance, short-term variations of the observed polarization may be analyzed. Alternatively, it could be applied to further investigate spatial variations of Venus' atmosphere properties. Also, absolute radiance measurements could be employed in such an analysis, provided that a recalibration of these data will become available. The method may further be extended to incorporate in a more advanced way the influence of measurement errors on the derived results, e.g., by employing Bayesian inference, as described by *Dolman et al.* [1992]. In the future, we intend to investigate the use of the method in its current state for the analysis of terrestrial polarization observations, such as are being obtained by the Global Ozone Monitoring Experiment (GOME) [*European Space Agency*, 1995], which flies on the ERS–2 mission, and POLDER [*Deschamps et al.*, 1994], which flies on the Advanced Earth Observing System (ADEOS) mission, and will be obtained by, e.g., Earth observing scanning polarimeter (EOSP) [*Travis*, 1992] which is scheduled for the EOS mission.

Our investigations of long-term variations gave the following results. Haze optical thicknesses were derived of about 0.25 in 1978 and of about 0.1 or less in 1990. Derived values during the years in between show significant short-term variations. However, after employing sliding averages to suppress short-term variations, we conclude that the derived haze optical thickness decreases during the Pioneer Venus mission. This conclusion is supported by a statistical analysis of the derived haze optical thicknesses. On the other hand, derived values of cloud top pressure and molecular absorption optical thickness within the main cloud deck at 270 nm vary irregularly about values of 15 mbar and 1.5, respectively, without indicating trends. We found only small correlations between the derived time variations of haze optical thickness, cloud-top pressure, and molecular absorption optical thickness.

A slight adjustment of haze particle sizes was found not to alter our main conclusions, but it did reduce the differences between haze optical thicknesses as derived from different wavelength combinations. The same thing occurred for the cloud-top pressures. The remaining differences, however, require further study. We confirm suggestions of *Sato et al.* [1996] that an increase of cloud-top pressure and a simultaneous decrease of haze optical thickness occurred in 1983. However, further investigations are needed for an explanation of the phase angle dependence of the polarization of Venus in that period.

Sato et al. [1996] derived short-term variations of the haze optical thickness near the poles. These variations are not directly linked to the variations that we deduced. Based on the following two arguments, we think that the changes that we found are mainly caused by variations in haze optical thickness at low latitudes.

(1) There is a considerable amount of haze at low latitudes, as shown by *Knibbe et al.* [1997].

(2) We estimate that the polar regions investigated by *Sato et al.* [1996] contribute less than 10% to the disk averages of q that we analyzed.

Such variations may be the reason that we infer a decrease in haze optical thickness, whereas *Sato et al.* [1996] do not report a trend of decreasing haze optical thickness. Therefore we expect that an analysis of spatial variations of haze optical thickness of maps later in the mission will show larger differences between poles and low latitudes than were found for maps early in the mission.

Sulfur dioxide is a precursor gas of haze and cloud particles in Venus' atmosphere [cf. *Winick and Stewart*, 1980; *Yung and Demore*, 1982; *Krasnopolsky and Pollack*, 1994]. A decrease of the sulfur dioxide concentration above Venus' cloud-top has been reported by *Na et al.* [1994], *Zasova et al.* [1993], *Na et al.* [1990], and *Esposito et al.* [1988]. This decrease was fast from 1979

to 1982 and slow from 1982 to 1990 [cf. *Na et al.*, 1994]. It coincides with the decrease in haze optical thickness that we found. A similar coincidence was noted first by *Esposito et al.* [1988]. However, it does not coincide with a decrease of the absorption optical thickness at 270 nm (expectedly caused by sulfur dioxide within the clouds), which we found to remain more or less constant. Apparently, globally averaged sulfur dioxide concentrations above and inside the clouds are not directly linked. Because polarization studies cannot be used to determine the sulfur dioxide concentrations above the clouds, it is recommended to include radiance observations at 270 nm to determine sulfur dioxide concentrations above and inside the clouds. Such a study might improve our understanding of the mechanisms involved in the evolution of the haze layer on Venus.

Acknowledgments. It is a pleasure to thank L. W. Esposito for constructive comments on an earlier version of this paper. This work has been supported in part by a Columbia University research program funded by NASA Goddard Institute for Space Studies.

References

Alms, G. R., A. K. Burnham, and W. H. Flygare, Measurements of the dispersion in the polarizability tensor, *J. Chem. Phys., 63*, 3321–3326, 1975.

Barker, E. S., J. H. Woodman, M. A. Perry, B. A. Hapke, and R. Nelson, Relative spectrophotometry of Venus from 3067 to 5960 Å, *J. Atmos. Sci., 32*, 1205–1211, 1975.

Bohren, C. F., and D. R. Huffman, *Absorption and Scattering of Light by Small Particles*, John Wiley, New York, 1983.

Chandrasekhar, S., *Radiative Transfer*, Oxford Univ. Press, New York, 1950.

Coffeen, D. L., and T. Gehrels, Wavelength dependence of the polarization. XV. Observations of Venus, *Astron. J., 74*, 433–445, 1969.

Coffeen, D. L., and J. E. Hansen, Polarization studies of planetary atmospheres, in *Planets, Stars and Nebulae Studied with Photopolarimetry*, edited by T. Gehrels, pp. 518–581, Univ. of Ariz. Press, Tucson, 1974.

Colin, L., The Pioneer Venus program, *J. Geophys. Res., 85*, 7575–7958, 1980.

Colin, L., and D. M. Hunten, Pioneer Venus experiment descriptions, *Space Sci. Rev., 20*, 451–525, 1977.

De Haan, J. F., Effects of aerosols on the brightness and polarization of cloudless planetary atmospheres, Ph.D. thesis, Free Univ., Amsterdam, The Netherlands, 1987.

De Haan, J. F., P. B. Bosma, and J. W. Hovenier, The adding method for multiple scattering calculations of polarized light, *Astron. Astrophys., 131*, 371–391, 1987.

De Rooij, W. A., and C. C. A. H. van der Stap, Expansion of Mie scattering matrices in generalized spherical functions, *Astron. Astrophys., 131*, 237–248, 1984.

Deschamps, P.–Y., F.–M. Bréon, M. Leroy, A. Podaire, A. Bricaud, J.–C. Buriez, and G. Sèze, The POLDER mission: Instrument characteristics and scientific objectives, *IEEE Trans. Geosci. Remote Sens., 32*, 598–615, 1994.

Dollfus, A., Contribution au Colloque Caltech–JPL sur la Lune et les Planètes: Vénus, in *Proceedings of Caltech–JPL Lunar and Planetary Conference, Rep. JPL TM 33–266*, pp. 187–202, Jet Propul. Lab., Pasadena, Calif., 1966.

Dollfus, A., and D. L. Coffeen, Polarization of Venus. I. Disk observations, *Astron. Astrophys., 8*, 251–266, 1970.

Dolman, V. L., J. F. de Haan, and J. W. Hovenier, *Bayesian linear analysis with application to removal of atmospheric influences on optical remote sensing images*, Rep. BCRS–92–19, Dutch Natl. Remote Sens. Board, Delft, The Netherlands, 1992.

Draper, N. R., and H. Smith, *Applied Regression Analysis*, John Wiley, New York, 1966.

Esposito, L. W., R. G. Knollenberg, M. Y. Marov, O. B. Toon, and R. B. Turco, The clouds and hazes of Venus, in *Venus*, edited by D. M. Hunten, L. Colin, T. M. Donahue, and V. I. Moroz, pp. 484–564, Univ. of Ariz. Press, Tucson, 1983.

Esposito, L. W., M. Copley, R. Eckert, L. Gates, A. I. F. Stewart, and H. Worden, Sulfur dioxide at the Venus cloud tops, 1978–1986, *J. Geophys. Res., 93*, 5267–5276, 1988.

European Space Agency, GOME users manual, *ESA SP–1182*, 1995.

Gunst, R. F., and R. L. Mason, *Regression Analysis and its Applications*, Marcel Dekker, New York, 1980.

Hansen, J. E., and J. W. Hovenier, Interpretation of the polarization of Venus, *J. Atmos. Sci., 31*, 1137–1160, 1974.

Hansen, J. E., and L. D. Travis, Light scattering in planetary atmospheres, *Space Sci. Rev., 16*, 527–610, 1974.

Hildebrand, F. B., *Introduction to Numerical Analysis*, Dover, New York, 1974.

Hovenier, J. W., and C. V. M. van der Mee, Fundamental relationships relevant to the transfer of polarized light in a scattering atmosphere, *Astron. Astrophys., 128*, 1–16, 1983.

Kawabata, K., Investigation of some of the principal geometric effects on planetary polarization, *Moon Planets, 24*, 291–381, 1981.

Kawabata, K., and J. E. Hansen, Interpretation of the variation of polarization over the disk of Venus, *J. Atmos. Sci., 32*, 1133–1139, 1975.

Kawabata, K., D. L. Coffeen, J. E. Hansen, W. A. Lane, M. Sato, and L. D. Travis, Cloud and haze properties from Pioneer Venus polarimetry, *J. Geophys. Res., 85*, 8129–8140, 1980.

Knibbe, W. J. J., J. F. de Haan, J. W. Hovenier, and L. D. Travis, A biwavelength analysis of Pioneer Venus polarization observations, *J. Geophys. Res., 102*, 10945–10958, 1997.

Krasnopolsky, V. A., and J. B. Pollack, H_2SO_4–H_2O System in Venus' clouds and OCS, CO, and H_2SO_4 profiles in Venus' troposphere, *Icarus, 109*, 58–78, 1994.

Lane, W. A., Wavelength dependence of the polarization. XXXV. Vertical structure of scattering layers above the visible Venus clouds, *Astron. J., 84*, 683–691, 1979.

Martonchik, J. V., and R. Beer, Analysis of spectrophotometric observations of Venus in the 3–4 μm region, *J. Atmos. Sci., 32*, 1151–1156, 1975.

Moroz, V. I., Stellar magnitude and albedo data of Venus, in *Venus*, edited by D. M. Hunten, L. Colin, T. M. Donahue, and V. I. Moroz, pp. 27–35, Univ. Ariz. Press, Tucson, 1983.

Na, C. Y., L. W. Esposito, and T. E. Skinner, International Ultraviolet Explorer observations of Venus SO_2 and SO, *J. Geophys. Res., 95*, 7485–7491, 1990.

Na, C. Y., L. W. Esposito, W. E. McClintock, and C. A. Barth, Sulfur dioxide in the atmosphere of Venus, *Icarus, 112*, 389–395, 1994.

Palmer, K. F., and D. Williams, Optical constants of sulfuric acid; application to the clouds of Venus?, *Appl. Opt., 14*, 208–219, 1975.

Pollack, J. B., O. B. Toon, R. Whitten, R. Boese, B. Ragent, M. Tomasko, L. Esposito, L. Travis, and D. Wiedman, Distribution and source of the UV absorption in Venus' atmosphere, *J. Geophys. Res., 85*, 8141–8150, 1980.

Polyak, I., *Computational Statistics in Climatology*, Oxford Univ. Press, New York, 1996.

Press, W. H., S. A. Teukolsky, W. T. Vetterling, and B. P. Flannery, *Numerical Recipes*, Cambridge Univ. Press, New York, 1992.

Ragent, B., L. W. Esposito, M. G. Tomasko, M. Y. Marov, V. P. Shari, and V. N. Lebedev, Particulate matter in the Venus atmosphere, *Adv. Space Res., 5*, 85–115, 1985.

Russell, E., L. Watts, S. Pellicori, and D. Coffeen, Orbiter cloud photopolarimeter for the Pioneer Venus mission, *Proc. Soc. Photo. Opt. Instrum. Eng., 112*, 28–44, 1977.

Santer, R., and M. Herman, Wavelength dependence of the po-

larization. XXXVIII. Analysis of ground-based observations of Venus, *Astron. J., 84*, 1802–1810, 1979.

Sato, M., L. D. Travis, and K. Kawabata, Photopolarimetry analysis of the Venus atmosphere in polar regions, *Icarus, 124*, 569-585, 1996.

Stoer, J., and R. Bulirsch, *Introduction to Numerical Analysis*, Springer Verlag, Berlin, 1993.

Tomasko, M. G., L. R. Doose, P. H. Smith, and A. P. Odell, Measurements of the flux of sunlight in the atmosphere of Venus, *J. Geophys. Res., 85*, 8167–8186, 1980.

Travis, L. D., On the origin of ultraviolet contrasts on Venus, *J. Atmos. Sci.*, 32, 1190–1200, 1975.

Travis, L. D., Earth observing scanning polarimeter, in Long Term Monitoring of Global Climate Forcings and Feedbacks, edited by J. Hansen, W. Rossow, and I. Fung, pp. 40–46, *NASA* Conf. Publ., CP-3234, 1992.

Van de Hulst, H. C., *Light Scattering by Small Particles*, John Wiley, New York, 1957.

Winick, J. R., and A. I. F. Stewart, Photochemistry of SO_2 in Venus' upper cloud layers, *J. Geophys. Res., 85*, 7849–7860, 1980.

Yung, Y. L., and W. B. Demore, Photochemistry of the stratosphere of Venus: Implications for atmospheric evolution, *Icarus, 51*, 199–247, 1982.

Zasova, L. V., V. I. Moroz, L. W. Esposito, and C. Y. Na, SO_2 in the middle atmosphere of Venus: IR measurements from Venera–15 and comparison to UV data, *Icarus, 105*, 92–109, 1993.

J. F. de Haan, and J. W. Hovenier, Department of Physics and Astronomy, Free University, De Boelelaan 1081, NL-1081 HV Amsterdam, Netherlands. (e-mail: johan@nat.vu.nl; hovenier@nat.vu.nl)

W. J. J. Knibbe, Transport Research Center (AVV), Ministry of Transport, Public Works and Water Management, P.O. Box 1031, NL-3000 BA Rotterdam, Netherlands. (e-mail: w.j.j.knibbe@avv.rws.minvenw.nl)

L. D. Travis, NASA Goddard Institute for Space Studies, 2880 Broadway, New York, NY 10025. (e-mail: pdldt@giss.nasa.gov)

(Received May 6, 1997; revised November 17, 1997;
accepted December 1, 1997.)